JOURNAL OF Materials CHEMISTRY

Structural changes of polyaniline/montmorillonite nanocomposites and their effects on physical properties

Dongkyu Lee,[a] Kookheon Char,*[a] Sang Wook Lee[b] and Yung Woo Park[b]

[a]*School of Chemical Engineering and Institute of Chemical Processes, Seoul National University, Seoul 151-744, Korea. E-mail: khchar@plaza.snu.ac.kr; Fax: +82-2-873-1548*
[b]*School of Physics and Condensed Matter Research Institute, Seoul National University, Seoul 151-747, Korea*

Received 24th March 2003, Accepted 29th August 2003
First published as an Advance Article on the web 9th September 2003

Polyaniline/montmorillonite (MMT) nanocomposites containing different PANI contents were prepared by the intercalation of aniline monomer into pristine MMT followed by the subsequent oxidative polymerization of the aniline in the interlayer spacings. The polyaniline/MMT nanocomposite structure intercalated with polyaniline (PANI) was examined by X-ray diffraction (XRD) and transmission electron microscopy (TEM). From the full-width at half-maximum (FWHM) of the (001) reflection peaks in the XRD patterns, the PANI/MMT nanocomposite containing 12.3 wt% PANI (PMN12) was found to be in the most disordered state. The physical interaction between the intercalated PANI and the basal surfaces of MMT was monitored by FT-IR. The room-temperature conductivity (σ_{RT}) varied from 9.1×10^{-9} to 1.5×10^{0} S cm^{-1} depending on the PANI content in the nanocomposites. The temperature dependence of dc conductivity ($\sigma_{dc}(T)$) of all the samples follows the quasi-1D variable range hopping (quasi-1D VRH) model (*i.e.*, $\sigma_{dc}(T) \propto \exp[-(T_0/T)^{1/2}]$). The charge transport behavior of this system was interpreted from the slopes (T_0) of the σ_{dc} curves and the highest T_0 value was found for the PANI/MMT nanocomposite with 12.3 wt% PANI (PMN12). The FT-IR, $\sigma_{dc}(T)$ and σ_{RT} results for the nanocomposites with varying content of PANI are consistently related to the structure of the PANI/MMT nanocomposites discussed in the XRD analysis. The structural argument was further supported by scanning electron microscopy (SEM) of all the samples. Thermogravimetric analysis (TGA) showed improved thermal stability for the intercalated nanocomposites in comparison with the pure PANI and a simple PANI/MMT mixture.

1. Introduction

Conducting polymer/layered inorganic solid nanocomposites have been the subject of considerable interest because, being derived from a unique combination of organic and inorganic components at the molecular level, they show novel electrical, structural and mechanical properties.[1,2] The two-dimensional (2-D) frameworks are typical of layered inorganic solids such as transition-metal oxides (V_2O_5, MoO_3), dichalcogenides (MoS_2), oxyhalides (FeOCl), halides (α-$RuCl_3$), phosphates ($Zr(HPO_4)_2$, $VOPO_4$), mica-type layered silicates (2 : 1 layered silicates, smectite clays) as well as layered double hydroxides (LDHs).[3–15] Among such 2-D inorganic materials, the layered silicates are the most common 2-D solids and their unique characteristics, such as high aspect ratio as well as high surface area, make an important contribution to novel properties of nanocomposites.[16,17] Layered silicates such as montmorillonites and hectorites possess the same structural characteristics as the well-known talc and mica.[18]

One of the most studied pairs in conducting polymer/layered inorganic solid nanocomposites are the nanocomposites composed of polyaniline (PANI) chains confined in the 2-D galleries of layered silicates with the unique characteristics mentioned above. After the observation of PANI intercalation into Cu^{2+}-exchanged silicates by Cloos *et al.* in 1979,[19] a number of studies on the preparation, properties and applications of PANI/layered silicate nanocomposites were carried out.[10–14,20–28] Most recently, Yang and Chen reported the synthesis of PANI/organically modified clay nanocomposites and found that more PANI chains are formed between interlayer spacings of the modified clay, especially for $HOOC(CH_2)_{11}NH_3^+$ modified clay because the acidic $HOOC(CH_2)_{11}NH_3^+$ ions residing between interlayer spacings provide a stronger driving force for the intercalation of aniline monomer.[29] Yeh *et al.* reported that regardless of clay content, the synthesis of PANI/clay nanocomposites with exfoliated silicate layers of clay was realized and they investigated the effect of such nanocomposites on the corrosion protection of cold rolled steel (CRS) when compared with that of an emeraldine base of PANI using a series of electrochemical measurements of corrosion potential and polarization resistance.[30] To our knowledge, however, systematic studies on the effect of structural variation induced by an increase in PANI content on the physical properties of PANI/layered silicate nanocomposites are yet to be done.

In the present paper, based on our previous work,[23] we further characterize the structure of PANI/MMT nanocomposites spanning the complete range of PANI content and perform more systematic studies on the effect of structural change on the physical properties, with special emphasis on the electrical properties, of nanocomposites using XRD, transmission electron microscopy (TEM), scanning electron microscopy (SEM), Fourier transform infrared spectroscopy (FT-IR), electrical conductivity measurements and thermogravimetric analysis (TGA).

2. Experimental

Materials

Aniline monomer (99%, Junsei) was dried over CaH_2 and distilled under reduced pressure prior to use. Hydrochloric acid (HCl) as a dopant and ammonium persulfate ($(NH_4)_2S_2O_8$, APS) as an oxidant were purchased from Junsei and used as received. Sodium montmorillonite (Na^+-MMT) with a cation

 DOI: 10.1039/b303235c

exchange capacity of 92 meq/100 g and a mean chemical formula of $Na_{0.65}[Al, Fe]_4Si_8O_{20}(OH)_2$ was employed as an inorganic material and supplied by Southern Clay Product.[31] The particle size of Na^+-MMT was found to be mostly below 13 μm.

Synthesis of PANI/MMT nanocomposites

PANI/MMT nanocomposites were prepared by the initial intercalation of aniline into Na^+-MMT and subsequent polymerization of aniline in the galleries.[11,12,23] A typical synthesis procedure for the preparation of PANI/MMT nanocomposites is as follows: Na^+-MMT was first introduced to a 1.5 M HCl aqueous solution with gentle stirring for 1 h. Aniline monomer was subsequently added to the colloidal suspension of Na^+-MMT until the aniline monomer was fully intercalated into the silicate layers of Na^+-MMT. Different weight ratios of aniline monomer to Na^+-MMT were used. Ammonium persulfate, dissolved in aqueous HCl of the same molarity, was slowly added dropwise to the mixture containing aniline monomer and Na^+-MMT. The reaction mixture was then stirred at 0 °C for 4 h. The final nanocomposites were isolated on a filter, thoroughly washed with distilled water and methanol and dried under vacuum at 70 °C for 3 days. The amount of PANI incorporated into the nanocomposites was determined gravimetrically and compared with that calculated from the weight loss of thermogravimetric analysis (TGA). As a reference for the intercalated nanocomposites, simple mixtures of PANI/MMT (*immiscible* composites) were also prepared by simply mixing PANI and Na^+-MMT with the same PANI content as that for the intercalated system.

Characterization

X-Ray diffraction (XRD) patterns were obtained with a Macscience-M18XHF instrument with a rotating anode and Ni-filtered Cu-Kα radiation ($\lambda = 0.154$ nm) operating at 50 kV and 100 mA. Transmission electron microscopy (TEM) was used to confirm the structure of the nanocomposites. For TEM observation, the ground fine powders of PANI/MMT nanocomposites were dispersed in ethanol and transferred to carbon coated Cu grids of 200 mesh. TEM was performed on a JEOL JEM-2000EXII using an accelerating voltage of 200 kV. The amount of sodium element in the PANI/MMT nanocomposites was analyzed by inductively coupled plasma-atomic emission spectroscopy (ICP-AES, Shimadzu ICPS-1000IV). Fourier-transform infrared spectroscopy (FT-IR) was carried out on the nanocomposites with a Nicolet-Impact 410 instrument using KBr pellets.

The variable-temperature electrical conductivities of the PANI/MMT nanocomposites were measured by the conventional dc four-probe method in a closed cycle cryogenic refrigerator after preparation of pressed pellets. Gold wires in a four-probe configuration were connected in parallel to the sample surface. The sample temperature was controlled using a LakeShore DRC-91C temperature system. The current was applied using a Keithley 224 programmable current source and the voltage drop was measured by a Keithley 2001 multimeter.

The morphologies of the nanocomposites with different PANI content were examined using scanning electron microscopy (SEM, JEOL JSM-840A) at 20 kV of accelerating voltage. The samples used for morphology examination were also prepared by compacting the nanocomposite powders into a pellet. The pressed specimens were then fractured in liquid nitrogen, and the fracture surface was sputtered with gold prior to observation. Thermogravimetric analysis (TGA) was carried out using a TA model 2050 TGA instrument under a nitrogen atmosphere at a heating rate of 10 °C min^{-1}. The residual weight of the samples (TGA curves) and their weight derivatives (DTG curves) as a function of temperature were recorded.

3. Results and discussion

Synthesis and structural characterization

Nanocomposites composed of the emeraldine salt form of PANI (PANI-ES) and MMT clays were prepared by the intercalation of aniline monomer into interlayer spacings of the MMT followed by the oxidative polymerization of aniline with ammonium persulfate.[11,12,23] In order to confirm the deintercalation of sodium cations out of the interlayer spacings of the MMT layers due to the intercalation of the aniline monomer, elemental analysis with ICP-AES was performed and the results are summarized in Table 1. The amount of sodium cation present in the nanocomposites was found to be negligible compared with the sodium amount in the pristine Na^+-MMT. As a result, we conclude that the interlayer sodium cations initially present in the Na^+-MMT have completely been replaced by aniline monomers. All the nanocomposites prepared in the present study will be hereafter denoted as PANI/MMT nanocomposites (PMN).

The X-ray diffraction (XRD) patterns and the full-width at half-maximum (FWHM, σ_q) of the (001) reflection peaks of PANI/MMT nanocomposites with different PANI contents as well as for the pristine Na^+-MMT are shown in Fig. 1. The *d*-spacings of the nanocomposites were estimated from the angular positions 2θ of the observed (001) reflection peaks based on the Bragg formula $\lambda = 2d\sin\theta$, where λ is the wavelength of the X-ray beam and θ is the scattering angle. As shown in Fig. 1A, the (001) reflection peak of the pristine Na^+-MMT at around $2\theta = 9°$ is shifted toward lower angles for all the nanocomposites regardless of the PANI content. The average *d*-spacing of the nanocomposites was found to be 1.43 nm with slight variation. Upon the intercalation of PANI, the interlayer spacing is expanded from 0.97 to 1.43 nm. In the case of the PANI/layered inorganic solid nanocomposites, the interlayer expansion generally varies in the range of 0.3 to 0.6 nm.[3–15] Thus, the 0.46 nm expansion in the interlayer spacing observed in this study indicates the insertion of PANI chains between silicate layers and is also comparable to the data reported by other groups.[5,11,14]

Table 1 Characteristics of polyaniline/MMT nanocomposites (PMN) prepared in this study

Sample	PANI content in PMN[a] (wt%)	Sodium content in PMN[b] (wt%)	*d*-spacing/nm	Mean crystallite size,[c], L/nm	Room-temp. conductivity[d], σ_{RT}/S cm^{-1}
Pristine Na^+-MMT	—	3.70	0.97	9.50	9.06×10^{-9}
PMN12	12.3	0.071	1.42	5.70	8.26×10^{-7}
PMN25	24.7	0.071	1.43	7.03	3.18×10^{-3}
PMN43	43.3	0.070	1.43	8.03	1.62×10^{-2}
PMN75	74.7	0.070	1.45	9.47	0.10
Pure PANI (PANI-ES)	100	—	—		1.51

[a]Determined by weight measurement. [b]Determined from inductively coupled plasma-atomic emission spectroscopy (ICP-AES). [c]Calculated from the Scherrer equation, $L = k\lambda(\sigma_q\cos\theta)$, where k is a constant, λ is the X-ray wavelength, σ_q is the full-width at half-maximum (FWHM) and θ is the scattering angle. [d]The reported σ_{RT} at each PANI content is the mean value of more than five measurements.

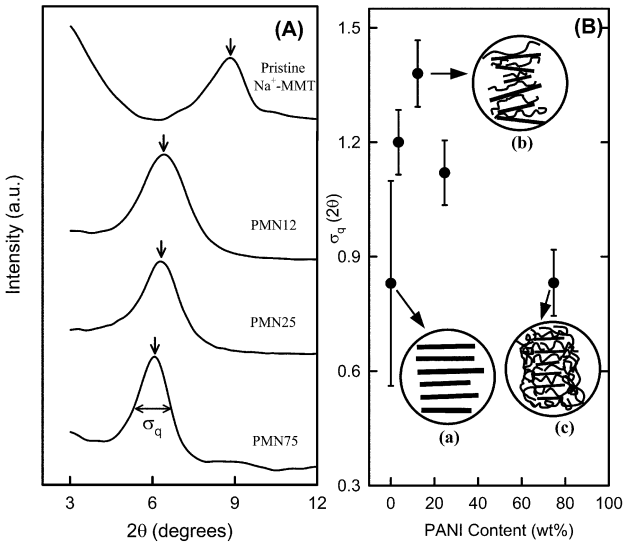

Fig. 1 (A) XRD patterns and (B) full-width at half-maximum (σ_q) of PANI/MMT nanocomposites as a function of PANI content. Schematics illustrating the change in the silicate arrays of MMT by the addition of PANI are also represented in (B).

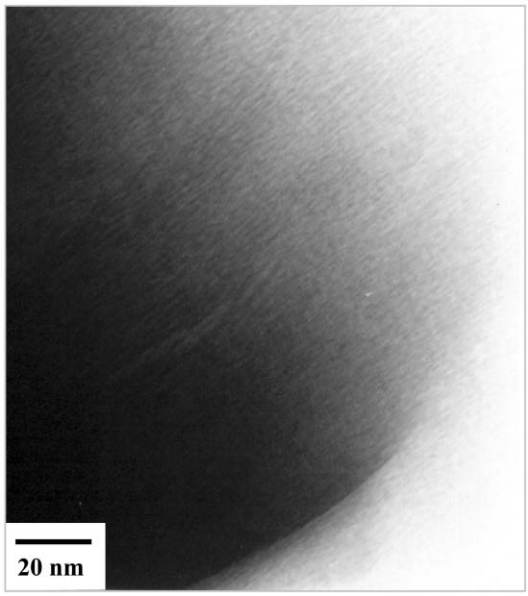

Fig. 2 TEM micrograph of PMN75.

It is also interesting to note in Fig. 1B that the FWHM's (σ_q) of the (001) reflection peaks clearly change for PANI/MMT nanocomposites with different amounts of PANI. The FWHM is a maximum for a PANI content of 12.3 wt% and then decreases at higher PANI content, finally approaching the FWHM value of the pristine Na^+-MMT. Since the FWHM provides a good measure of the expansion distribution of the basal spacing of silicate layers through the Scherrer equation, $L = k\lambda/(\sigma_q \cos\theta)$,[32–35] schematics illustrating the degree of order in the arrays of silicate layers in nanocomposites with different amounts of PANI are also given in Fig. 1B. From the σ_q values of the XRD patterns, the crystallite sizes (L) for all the nanocomposites as well as for the pristine Na^+-MMT can be calculated using the Scherrer equation and are presented in Table 1. The maximum σ_q (*i.e.*, the minimum L) at a PANI content of 12.3 wt% indicates that the intercalation of a given amount of PANI chains into the silicate layers causes the most disordered arrays of silicate layers (*i.e.*, (b) in Fig. 1B). Above 12.3 wt% PANI content in the nanocomposites, the basal surface of the silicate layers is fully saturated with the PANI chains and the excess PANI chains (*i.e.*, *free* PANI chains) are expected to reside outside the interlayer region ((c) in Fig. 1B).

The structures of the nanocomposites intercalated with PANI were also confirmed by TEM observations. Fig. 2 shows a TEM micrograph of PMN75 (a nanocomposite containing 74.7 wt% of PANI), in which the dark lines are the silicate layers of MMT. As shown in Fig. 2, the lamellar stacks (*i.e.*, the multilayered morphology) are clearly observed. This is direct evidence for PANI being intercalated into the interlayer spacings of the silicate layers in the nanocomposites.

Fig. 3 shows FT-IR spectra of pristine Na^+-MMT, pure PANI (PANI-ES), a PANI/MMT simple mixture (*i.e.*, an *unintercalated* system) and a PANI/MMT nanocomposite (*i.e.*, an *intercalated* system) with the same amount of PANI. Characteristic bands corresponding to pristine Na^+-MMT are shown at 1030 (ν(Si–O)), 914 (δ(Al–OH)) and 520 cm^{-1} (ν(Si–O–Al)).[36] In addition, the FT-IR spectrum of pure PANI shows four major vibration bands at 1112 (*para*-substituted aromatic δ(C–H) in plane), 1296 (ν(C–N)), 1477 (benzenoid ring ν(C=C)) and 1562 cm^{-1} (quinoid ring ν(C=C)) and these observed bands are in good agreement with previously published values.[37,38] For the intercalated nanocomposite and the simple mixture having the same amount (12.3 wt%) of PANI, the FT-IR spectra show characteristic bands of pure PANI, as mentioned above, indicating the existence of PANI in the emeraldine salt form (PANI-ES). However, we note from a closer look at the spectra that there is a slight difference, as shown in Figs. 3c and 3d. The band at 1296 cm^{-1} for the simple mixture and PANI-ES, assigned as the stretching vibration of C–N (ν(C–N)) as indicated by a thick arrow in Fig. 3b, is significantly shifted to 1311 cm^{-1} for the intercalated nanocomposite as shown in Fig. 3d.

It is well known that in systems intercalated with PANI, strong guest–host interactions, such as hydrogen bonding, occur in the form of NH···O=V in V_2O_5 and NH···Cl in FeOCl.[3,6] Chen and Hwang reported the formation of hydrogen bonds between hydroxyl groups and amines, charged amines or imine sites in the case of a blend between sulfuric acid ring-substituted polyaniline (SPAN) and poly(vinyl alcohol)

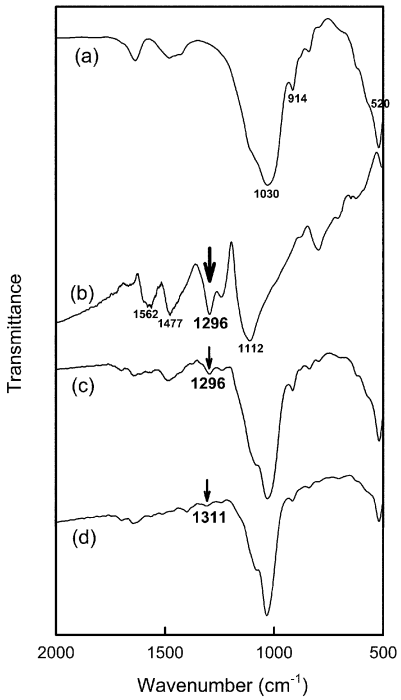

Fig. 3 FT-IR spectra of (a) pristine Na^+-MMT, (b) PANI-ES, (c) PANI/Na^+-MMT simple mixture with 12.3 wt% PANI, and (d) PANI/MMT nanocomposite with 12.3 wt% PANI.

and showed that the $C_{aromatic}$–N stretching of the SPAN with a 2 cm^{-1} shift to 1303 cm^{-1} is due to the hydrogen bonding.[39] Stutzmann and Siffert also reported similar results for the adsorption of acetamide molecules on clays.[40] Consequently, the frequency shift of ν(C–N) observed in our nanocomposite system is also believed to be caused by the physical interaction between PANI and the basal surface of MMT clay (*i.e.*, NH···O hydrogen bonding).

Electrical conductivity

Fig. 4A shows the temperature dependence of dc conductivity (σ_{dc}) of PANI/MMT nanocomposites with different PANI contents as well as of pure PANI-ES. The temperature-dependent conductivity was measured for all the samples from 300 K to 30 K except for a nanocomposite containing 12.3 wt% PANI (PMN12), which showed negligible conductivity ($<\exp(-19)$ S cm^{-1}) at temperatures below 200 K. It is noted that the dc conductivity of the nanocomposites decreases with a decrease in temperature, indicating typical semiconducting behavior.

In general, the temperature dependence of σ_{dc} for polyaniline is known to follow the quasi one-dimensional variable range hopping (quasi-1D VRH) model given by:[41,42]

$$\sigma_{dc} = \sigma_0 \exp\left[-\left(\frac{T_0}{T}\right)^{1/2}\right] \quad (1)$$

where σ_0 is the infinite temperature conductivity and T_0 is the effective energy barrier for electrons to hop between localized states and can be written as $T_0 = \frac{16\alpha}{zN(E_F)k_B}$ where α^{-1} is the localization length, $N(E_F)$ is the density of states at the Fermi level, k_B is the Boltzmann constant and z is the number of nearest-neighboring chains. As shown in Fig. 4A, the temperature dependence of σ_{dc} for all the nanocomposite samples containing pure PANI is well described by the relation $\sigma_{dc}(T) \propto \exp[-(T_0/T)^{1/2}]$. The T_0 values are extracted from the slopes of the lines in Fig. 4A and are plotted against PANI content in the nanocomposites in Fig. 4B. In the case of pure PANI-ES, the T_0 value of about 6400 K is in good agreement with the value reported in a previous study.[43] Surprisingly, among all the nanocomposites examined, PMN12 shows the highest T_0 value. Since T_0 is inversely proportional to the localization length ($1/\alpha$), this result indicates that PMN12 reflects much greater electron localization than other nanocomposites. Unlike pure PANI, the electrical conductivity of PANI/layered silicate (clay) nanocomposites depends on the nature of both the host clay and the guest PANI. In this context, for the intercalated nanocomposites containing isolated molecular PANI chains, the conductivity is lower than that of the corresponding pure PANI because of the existence of individual silicate layers with insulating character, which can screen the interchain interactions between PANI chains (*i.e.*, the shielding effect of silicates). Although a strong dependence of the T_0 value on the protonation level or the doping level ($[H^+]/[N]$ or $[Cl^-]/[N]$) exists,[43] in our case, the protonation level can be excluded by equilibrating the samples with a 1.5 M HCl solution. Consequently, it can be inferred from the T_0 value that at 12.3 wt% PANI, the insulating character of the silicate layers, which restricts the effective delocalization of charge carriers in the nanocomposites, becomes the most dominant because most of the PANI chains are intercalated into the interlayer spacings of MMT.

It should also be noted that the room-temperature conductivity (σ_{RT}) of PANI/MMT nanocomposites varies from 9.1×10^{-9} to 1.5×10^{0} S cm^{-1} depending on the PANI content, as shown in Fig. 5. In addition, there exists a rapid increase in σ_{RT} around 12.3 wt% PANI and σ_{RT} then gradually increases upon increasing the PANI content in the nanocomposites to more than 20 wt%. It appears that this trend in σ_{RT} indicates the typical percolation threshold at a PANI weight fraction showing the sudden increase in σ_{RT}. In order to carefully investigate the electrical conductivity of the nanocomposites, besides the shielding effect of silicates discussed above, the fact that the connectivity of PANI chains between different stacks of silicate layers can also affect the electrical conductivity should be taken into account. This connectivity can give rise to longer carrier paths and better electrical communication between the stacks.[3,12] As a consequence, based on the fact discussed in the XRD data that above 12.3 wt% PANI content, PANI chains intercalated between the

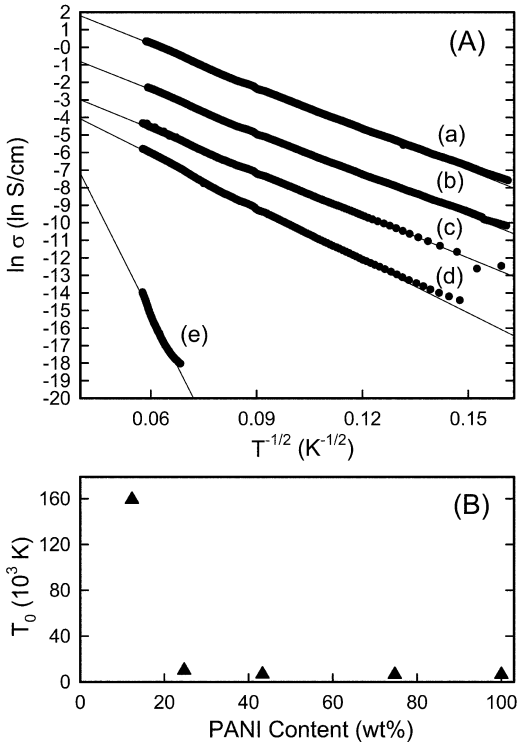

Fig. 4 (A) Temperature dependence of σ_{dc} and (B) effective energy barrier for electron hopping (T_0) in PANI/MMT nanocomposites as a function of PANI content: (a) PANI-ES, (b) PMN75, (c) PMN43, (d) PMN24, and (e) PMN12.

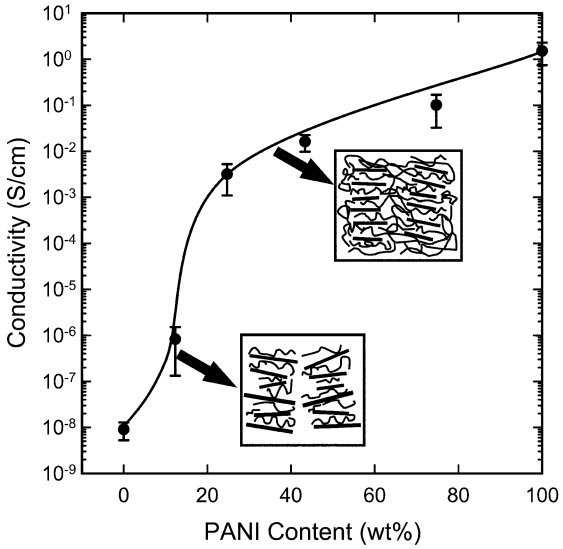

Fig. 5 Room-temperature conductivity (σ_{RT}) of PANI/MMT nanocomposites as a function of PANI content. Schematics representing expected morphologies for two different PANI contents are also given in the figure.

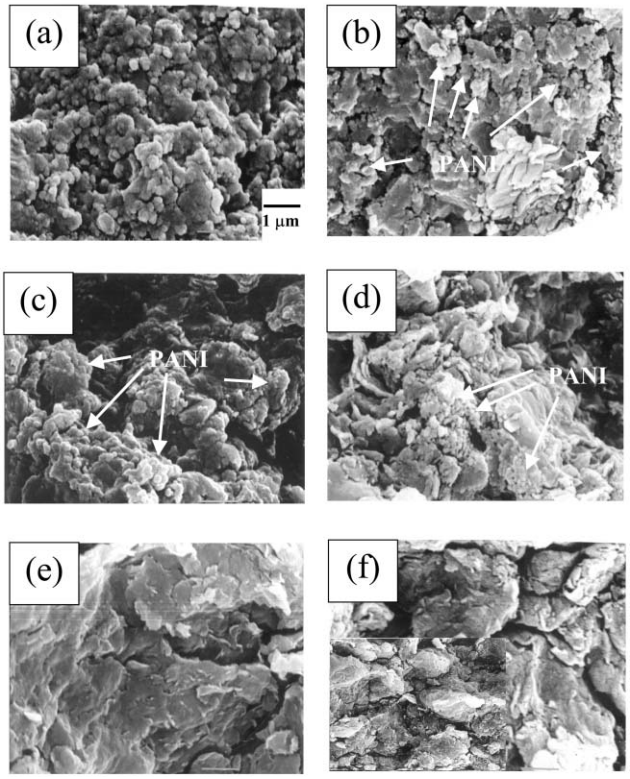

Fig. 6 SEM micrographs of PANI/MMT nanocomposites as a function of PANI content: (a) PANI-ES, (b) PMN75, (c) PMN43, (d) PMN25, (e) PMN12, and (f) pristine Na^+-MMT.

silicate layers and free PANI chains outside the silicate layers coexist, we conclude that the sudden increase in the conductivity at around 12.3 wt% PANI is induced by the presence of free PANI chains which facilitate the electron transfer between the intercalated PANI chains presumably due to the connectivity of free PANI chains, as illustrated in the inset of Fig. 5.

Morphology of PANI/MMT nanocomposites

To confirm the relationship between the electrical properties and the proposed structures of nanocomposites, SEM measurements were carried out for the same samples used for the electrical conductivity measurements. Fig. 6 shows SEM micrographs of PANI/MMT nanocomposites with different amounts of PANI in the nanocomposites. From the SEM micrographs, PANI-ES has a granular texture (*i.e.*, clusters of globules as shown in Fig. 6a) and pristine Na^+-MMT has a flaky texture reflecting its layered structure (Fig. 6f).[44,45] It can be clearly seen in Figs. 6b–e that textures of both PANI-ES and pristine Na^+-MMT are retained in the nanocomposites. As the PANI content is decreased, the characteristic granular texture of PANI-ES, indicated by white arrows in Figs. 6b–d, gradually disappear and the morphology of PMN12 (Fig. 6e) is quite similar to that of pristine Na^+-MMT. It should also be noted here that most of the PANI chains are intercalated into the interlayer spacings of MMT for PMN12 based on the XRD data. As a result, this SEM data strongly support the fact that the PANI chains shown in Figs. 6b–d (*i.e.*, free PANI domains) play an important role in the electrical conductivity of the nanocomposites.

Thermal analysis

Fig. 7 shows the thermogravimetric analysis curves (TGA curves) and corresponding derivative curves (DTG curves, inset) for pristine Na^+-MMT, pure PANI (PANI-ES) and PMN75. First, TGA mainly serves as an analytical technique to

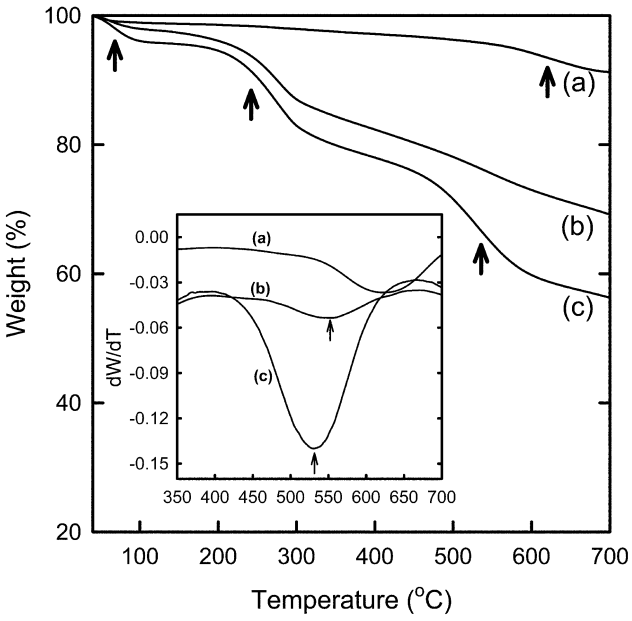

Fig. 7 TG and DTG (shown in the inset) curves of (a) pristine Na^+-MMT, (b) PMN75, and (c) PANI-ES as a function of temperature.

quantify the amount of organic matter (*i.e.*, PANI-ES in this study) in the PANI/MMT nanocomposites. Based on the weight loss of 32.7% for pure PANI-ES, the TGA weight loss for the nanocomposite (weight loss of 31%) is very close to the percentage of PANI-ES determined gravimetrically (weight measurement). Secondly, the TGA analysis was carried out to study the thermal stability of the nanocomposites. In general, the thermal behavior of pristine Na^+-MMT and pure PANI shows two- and three-step weight loss processes, respectively, as can be seen by the thick arrows in the TGA curve, indicating the majority weight loss for each step (Fig. 7a and c).[18,46,47]

In order to carefully compare the thermal behavior of a nanocomposite (intercalated system) with that of the PANI-ES, the DTG curves are shown in the inset of Fig. 7. Note that the temperature at the minimum of the DTG curve for the PANI-ES is nearly the same as that for a simple mixture with the same PANI content as intercalated system (PANI content of 74.7 wt%) at 530.6 °C (data not shown), which can be attributed to the thermal decomposition of pure PANI backbone chains, while the minimum temperature in the case of the PANI/MMT nanocomposite is shifted to a higher temperature by 25 °C, as indicated by the thin arrows in the inset of Fig. 7. It can be inferred from this result that the intercalated nanocomposite system is more thermally stable than the PANI-ES and the simple mixture. Lee *et al.*[48] investigated the thermal stability of aliphatic polyimide (PEI-10)/clay nanocomposites. They found that an immiscible PEI/clay mixture (*i.e.*, conventional mixture) containing the same amount of silicate as the intercalated nanocomposites showed no enhancement in thermal stability. This result is in good agreement with the data presented in our study. Burnside and Giannelis[49] also reported results similar to the present work for polydimethylsiloxane (PDMS)/layered silicate nanocomposites. Consequently, from the difference in decomposition temperature from the DTG curves shown in Fig. 7, it is suggested that for the intercalated nanocomposites, the silicate layers (nanolayers) with a high aspect ratio (100–1000) are believed to effectively act as barriers, blocking the degradation of PANI chains located between the interlayer spacings.

4. Conclusion

A series of PANI/MMT nanocomposites have been prepared by the intercalation of aniline monomer into interlayer spacings

of MMT, followed by oxidative polymerization. The structure–property relationship of these nanocomposites was investigated by a combination of XRD, TEM, SEM, FT-IR, electrical conductivity measurement and TGA.

From XRD and TEM, the intercalation of PANI into interlayer spacings of silicate layers is clearly confirmed. The change in the arrays of silicate layers in PANI/MMT nanocomposites upon increasing the amount of PANI was evaluated from the analysis of the full-width at half-maximum (FWHM) of the XRD patterns. It is also evident from the FT-IR spectra that there are physical interactions between the intercalated PANI chains and the MMT layers. The room-temperature conductivity (σ_{RT}) varies from 9.1×10^{-9} to 1.5×10^{0} S cm^{-1} and the temperature dependence of σ_{dc} was well represented by the quasi-1D VRH model. The value of T_0 from the model dramatically increases at around 12.3 wt% PANI content. We believe that this is related to the fact that the insulating effect of the silicate layers, which blocks the interchain interactions between individual PANI chains, is at a maximum for a nanocomposite containing 12.3 wt% PANI (*i.e.*, most of the PANI chains are intercalated into the clay). This result was further verified by SEM for all the nanocomposites. Based on the DTG curves in thermogravimetric analysis (TGA), the PANI chains in the PANI/MMT nanocomposites are more thermally stable than those of pure PANI (PANI-ES) and a simple mixture of PANI and MMT.

Acknowledgements

We are very grateful for the financial support from the National Research Laboratory Fund from the Ministry of Science and Technology (MOST), the Korean Ministry of Education through the Brain Korea 21 Program, and the Research Institute of Advanced Materials (RIAM) at Seoul National University. We also thank Mrs Mee Jeong Kang for her kind SEM and TEM measurements.

References

1 (*a*) S. D. Cox and G. D. Stucky, *J. Phys. Chem.*, 1991, **95**, 710; (*b*) P. Enzel and T. Bein, *J. Phys. Chem.*, 1989, **93**, 6270; (*c*) E. Ruiz-Hitzky, *Adv. Mater.*, 1993, **5**, 334.
2 (*a*) P. Enzel and T. Bein, *Chem. Mater.*, 1992, **4**, 819; (*b*) J. E. Pillion and M. E. Thompson, *Chem. Mater.*, 1991, **3**, 777; (*c*) L. F. Nazar, Z. Zhang and D. Zinkweg, *J. Am. Chem. Soc.*, 1992, **114**, 6239.
3 (*a*) M. G. Kanatzidis, C.-G. Wu, H. O. Marcy and C. R. Kannewurf, *J. Am. Chem. Soc.*, 1989, **111**, 4139; (*b*) C.-G. Wu, D. C. DeGroot, H. O. Marcy, J. L. Schindler, C. R. Kannewurf, Y. J. Liu, W. Hirpo and M. G. Kanatzidis, *Chem. Mater.*, 1996, **8**, 1992.
4 T. A. Kerr, H. Wu and L. F. Nazar, *Chem. Mater.*, 1996, **8**, 2005.
5 M. G. Kanatzidis, R. Bissessur, D. C. DeGroot, J. L. Schindler and C. R. Kannewurf, *Chem. Mater.*, 1993, **5**, 595.
6 M. G. Kanatzidis, C.-G. Wu, H. O. Marcy, D. C. DeGroot, C. R. Kannewurf, A. Kostikas and V. Papaefthymiou, *Adv. Mater.*, 1990, **2**, 364.
7 C.-G. Wu, D. C. DeGroot, H. O. Marcy, J. L. Schindler, C. R. Kannewurf, T. Bakas, V. Papaefthymiou, W. Hirpo, J. P. Yesinowski, Y. J. Liu and M. G. Kanatzidis, *J. Am. Chem. Soc.*, 1995, **117**, 9229.
8 L. Wang, P. Brazis, M. Rocci, C. R. Kannewurf and M. G. Kanatzidis, *Chem. Mater.*, 1998, **10**, 3298.
9 (*a*) G. E. Matsubayashi and H. Nakajima, *Chem. Lett.*, 1993, 423; (*b*) A. de Stefanis, S. Foglia and A. A. G. Tomlinson, *J. Mater. Chem.*, 1995, **5**, 475.
10 V. Mehrotra and E. P. Giannelis, *Solid State Ionics*, 1992, **51**, 115.
11 T.-C. Chang, S.-Y. Ho and K.-J. Chao, *J. Chin. Chem. Soc.*, 1992, **39**, 209.
12 Q. Wu, Z. Xue, Z. Qi and F. Wang, *Polymer*, 2000, **41**, 2029.
13 J. W. Kim, S. G. Kim, H. J. Choi and M. S. Jhon, *Macromol. Rapid Commun.*, 1999, **20**, 450.
14 H. Inoue and H. Yoneyama, *J. Electroanal. Chem.*, 1987, **233**, 291.
15 T. Challier and R. C. T. Slade, *J. Mater. Chem.*, 1994, **4**, 367.
16 T. J. Pinnavaia, *Science*, 1983, **220**, 365.
17 (*a*) P. B. Messersmith and E. P. Giannelis, *Chem. Mater.*, 1994, **6**, 1719; (*b*) K. Yano, A. Usuki, T. Kurauchi and O. Kamigaito, *J. Polym. Sci., Part A: Polym. Chem.*, 1993, **31**, 2493.
18 R. E. Grim, *Clay Mineralogy*, McGraw-Hill, New York, 1953.
19 P. Cloos, A. Moreale, C. Braers and C. Badot, *Clay Miner.*, 1979, **14**, 307.
20 V. Mehrotra and E. P. Giannelis, *Solid State Commun.*, 1991, **77**, 155.
21 H. L. Frisch, B. Xi, Y. Qin, M. Rafailovich, N. L. Yang and X. Yan, *High Perform. Polym.*, 2000, **12**, 543.
22 M. Biswas and S. S. Ray, *J. Appl. Polym. Sci.*, 2000, **77**, 2948.
23 D. Lee, S.-H. Lee, K. Char and J. Kim, *Macromol. Rapid Commun.*, 2000, **21**, 1136.
24 K. A. Carrado and L. Xu, *Chem. Mater.*, 1998, **10**, 1440.
25 T. L. Porter, D. Thompson, M. Bradley, M. P. Eastman, M. E. Hagerman, J. L. Attuso, A. E. Votava and E. D. Bain, *J. Vac. Sci. Technol. A.*, 1997, **15**, 500.
26 T. L. Porter, M. P. Eastman, D. Y. Zhang and M. E. Hagerman, *J. Phys. Chem. B*, 1997, **101**, 11106.
27 G. M. do Nascimento, V. R. L. Constantino and M. L. A. Temperini, *Macromolecules*, 2002, **35**, 7535.
28 B.-H. Kim, J.-H. Jung, S.-H. Hong, J. Joo, A. J. Epstein, K. Mizoguchi, J. W. Kim and H. J. Choi, *Macromolecules*, 2002, **35**, 1419.
29 S. M. Yang and K. H. Chen, *Synth. Met.*, 2003, **135-136**, 51.
30 J.-M. Yeh, S.-J. Liou, C.-Y. Lai and P.-C. Wu, *Chem. Mater.*, 2001, **13**, 1131.
31 W. Xie, Z. Gao, W.-P. Pan, D. Hunter, A. Singh and R. Vaia, *Chem. Mater.*, 2001, **13**, 2979.
32 G. W. Brindley and G. Brown, *Crystal Structures of Clay Minerals and Their X-ray Identification*, Mineralogical Society, London, 1980.
33 R. Limary, S. Swinnea and P. F. Green, *Macromolecules*, 2000, **33**, 5227.
34 P. Maiti, K. Yamada, M. Okamoto, K. Ueda and K. Okamoto, *Chem. Mater.*, 2002, **14**, 4654.
35 (*a*) B. E. Warren, *X-ray Diffraction*, Dover Publications, New York, 1990; (*b*) V. A. Dritis and C. Tchoubar, *X-ray Diffraction by Disordered Lamellar Structures*, Springer-Verlag, New York, 1990.
36 (*a*) V. Stubian and R. Roy, *J. Am. Ceram. Soc.*, 1961, **44**, 625; (*b*) J. A. Gadsden, *Infrared Spectra of Minerals and Related Inorganic Compound*, Butterworth, London, 1975.
37 (*a*) I. Harada, Y. Furukawa and F. Ueda, *Synth. Met.*, 1989, **29**, E303; (*b*) Y.-J. Liu and M. G. Kanatzidis, *Inorg. Chem.*, 1993, **32**, 2989.
38 (*a*) Y. Furukawa, F. Ueda, Y. Hyodo, I. Harada, T. Nakajima and T. Kawagoe, *Macromolecules*, 1988, **21**, 1297; (*b*) Y. H. Kim, C. Foster, J. Chiang and A. J. Heeger, *Synth. Met.*, 1988, **26**, 49.
39 S.-A. Chen and G.-W. Hwang, *Polymer*, 1997, **38**, 3333.
40 Th. Stutzmann and B. Siffert, *Clays Clay Miner.*, 1977, **25**, 392.
41 (*a*) Z. H. Wang, C. Li, E. M. Scherr, A. G. MacDiarmid and A. J. Epstein, *Phys. Rev. Lett.*, 1991, **66**, 1745; (*b*) N. F. Mott and E. A. Davis, *Elctronic Processes in Non-Crystalline Materials*, Clarendon Press, Oxford, 1979.
42 (*a*) Z. H. Wang, H. H. S. Javadi, A. Ray, A. G. MacDiarmid and A. J. Epstein, *Phys. Rev. B*, 1990, **42**, 5411; (*b*) Z. H. Wang, E. M. Scherr, A. G. MacDiarmid and A. J. Epstein, *Phys. Rev. B*, 1992, **45**, 4190.
43 F. Zuo, M. Angelopoulos, A. G. MacDiarmid and A. J. Epstein, *Phys. Rev. B*, 1987, **36**, 3475.
44 M. Wan, M. Li, J. Li and Z. Liu, *J. Appl. Polym. Sci.*, 1994, **53**, 131.
45 S. Sivakumar, A. D. Damodaran and K. G. K. Warrier, *Ceram. Int.*, 1995, **21**, 85.
46 S. Moreau, V. Balek and F. Béguin, *Mater. Res. Bull.*, 1999, **34**, 503.
47 (*a*) A. Wolter, P. Rannou, J. P. Travers, B. Gilles and D. Djurado, *Phys. Rev. B*, 1998, **58**, 7637; (*b*) J. Yue, A. J. Epstein, Z. Zhong and P. K. Gallagher, *Synth. Met.*, 1991, **41-43**, 765; (*c*) Y. Wei and K. F. Hsueh, *J. Polym. Sci., Part A: Polym. Chem.*, 1989, **27**, 4351; (*d*) K. Pielichowski, *Solid State Ionics*, 1997, **104**, 123.
48 J. Lee, T. Takekoshi and E. P. Gainnelis, *Mater. Res. Soc. Symp. Proc.*, 1997, **457**, 513.
49 S. D. Burnside and E. P. Giannelis, *Chem. Mater.*, 1995, **7**, 1597.